Appl. Phys. B 33, 29–41 (1984)

Applied Physics B Photophysics and Laser Chemistry

Investigation of Stimulated Brillouin Scattering Under Well-Defined Interaction Conditions

Part II. Experimental Results and Interpretation

B. Gellert* and B. Kronast

Institut für Experimentalphysik V, Ruhruniversität, D-4630 Bochum, Fed. Rep. Germany

Received 30 June 1983/Accepted 29 August 1983

Abstract. The spatial and temporal development of the SBS ion wave was investigated extensively by ruby-laser light scattering techniques using a picosecond streak-camera for recording. The measurements performed for various levels of peak backscattering provide the ion wave energy density as a function of space, time and backscatter level, i.e. peak power density of CO_2 laser radiation focussed into an underdense and homogeneous target plasma of large extent. In an attempt to understand the various experimental aspects, numerical solutions of respective theories were compared with observations. Whilst for backscatter levels below 5% the three-wave description of Forslund et al. [11] does suffice, it took an extensive review of nonlinear mechanisms to pin down harmonic production of the ion wave according to Karttunen and Salomaa [23] as the process governing SBS behaviour above 5% up to the Manley-Rowe limit. The corresponding system of four-wave equations is capable to explain reasonably well all the aspects observed; in particular, it shows, how it comes about that the dangerous Manley-Rowe limit is reached already at moderate power densities below 10^{13} W/cm^2 such as in [1]. From this description, it is also evident that – by contrast to many other aspects of laser fusion – this is an effect which becomes the more serious the *shorter* the laser wavelength is.

PACS: 52.35 Fp, 52.35 Mw, 52.35 Py

Stimulated Brillouin Scattering (SBS) has found great interest in laser plasma interaction studies with the future aim of an inertially confined fusion reactor. In particular, the expanding corona of the hot imploding plasma nucleus is an extended underdense homogenous plasma that should give rise to high backscatter, theoretically. In a model experiment, designed to follow closely theoretical assumptions of homogeneous plasma theory, the maximum Manley Rowe limit of near 100% backscattered radiation could be verified, recently [1].

In the last years, a controverse discussion of saturation effects with SBS has arisen leading even to contradictary results [2–6]. The main reason for these contradictions is – among others –, that the plasma parameters during the interaction with the exciting laser are not known with the precision necessary.

This paper deals with experiments which have been done under well-defined plasma conditions and might therefore be capable of a comparison with theoretical models. The experimental means for investigating the SBS behaviour was Thomson scattering at the CO_2 laser excited ion acoustic wave with a ruby-laser.

1. Experimental Arrangement

As a target plasma, the extended homogeneous plasma of a 25 kJ Z-pinch device was used, which had been diagnozed with great care [7]. The spatial density distribution is shown in Fig. 1. As can be seen, the target is a large homogenous plasma which is underdense for CO_2 laser radiation. Within the plasma diameter of approximately 20 mm an electron number densi-

* This author is now with Brown Boveri & Cie, Research Centre, CH-5405 Baden-Dättwil, Switzerland

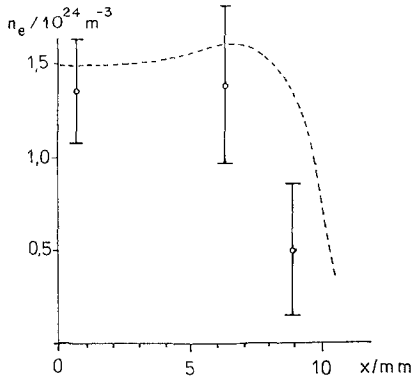

Fig. 1. Spatial density distribution of the target plasma at the time of maximum compression. The experimental values are taken from measurements of spectrally integrated light scattering measurements [7d], the dashed line was determined spectroscopically [7a]

ty n_e of $1.6 \times 10^{24}\ m^{-3}$ is found. The electron temperature of the homogeneous region is $k_B T_e = (11 \pm 3.5)$ eV, ion temperature $k_B T_i = (10.5 \pm 1.5)$ eV. The plasma is at rest for more than 50 ns [7d].

Stimulated Brillouin scattering was excited by means of a GW-CO_2 laser system of highest beam quality. The laser was also investigated thoroughly [8]. Making use of injection mode-locking the system delivered power densities of $10^{17}\ W/m^2$ with 1–2 ns duration.

By synchronizing a nanosecond ruby-laser with the CO_2 laser an experiment was performed by which a theoretical model describing heating of the plasma and heat conduction from the interaction volume could be confirmed [7d]. The cavity-dumped ruby-laser system delivered output power in excess of 100 MW within a 5 ns pulse of 2 mrad divergence. The mentioned simultaneous Thomson scattering experiment also proved, that the interaction conditions of the CO_2 laser experiment were well-defined and known during every phase of the interaction.

At first, the location of the SBS interaction volume should be found. The experimental set-up for this investigation is shown in Fig. 2. After passing the beam splitter BS and being reflected by mirror M1, the ring shaped CO_2 laser emission is focussed diffraction limited into the plasma by means of a plane convex lens L1 of 714 mm focal length. The incident radiation is monitored on a photon drag detector PD by the intensity reflected from the beamsplitter, which is focussed by lens L3 on to the detector after reflection from mirrors M2 and M3. The same detector is also used for monitoring backscattered light from the plasma.

The ruby-laser system illuminates the beam waist of the CO_2 laser inside the plasma by focussing the 6943 Å radiation into the plasma by means of lens L2 of 1 m focal length. According to **k**-matching conditions of Fig. 3, 7° forward scattering results for Thomson scattering at the excited ion acoustic wave with its wave-vector $\mathbf{k}_{ia} \approx 2\mathbf{k}_{CO_2}$, where $\mathbf{k}_{CO_2}$ is the wave-vector of the 10.6 μm CO_2 laser. Details can be found in [7d]. Lens L4 in Fig. 2 is used to image the CO_2 laser beam waist on to the entrance slit of a Hamamatsu streak camera system. When precise

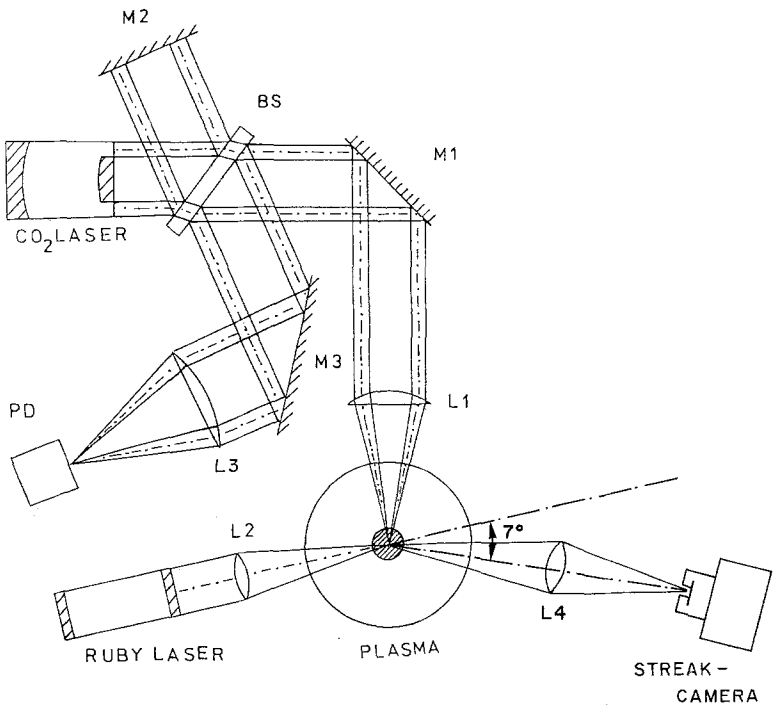

Fig. 2. Experimental set-up for the investigation of the SBS excited ion acoustic wave. For details see text. (M1, M2, M3: mirrors, L1, L2, L3, L4: lenses, BS: beam splitter, and PD: photon drag detector)

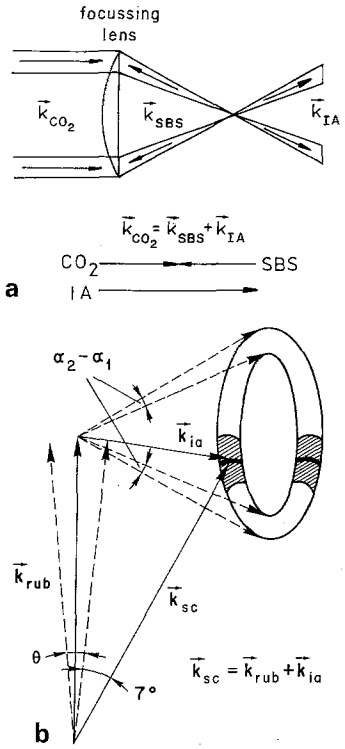

Fig. 3. (a) *k*-matching conditions of the SBS process. The ring shaped emission of the CO_2 laser is focussed into the plasma giving rise to a conical distribution of ion acoustic vectors $\mathbf{k}_{ia}$ and backscattered light $\mathbf{k}_{SBS}$. (b) *k*-matching conditions of the Thomson scattering process. Ruby-laser light ($\mathbf{k}_{rub}$) is scattered only at those ion acoustic vectors $\mathbf{k}_{ia}$ of the conical distribution that fulfil the matching condition $\mathbf{k}_{sc} = \mathbf{k}_{rub} + \mathbf{k}_{ia}$. Because of divergence of the incident radiation not only those vectors $\mathbf{k}_{ia}$ ending on the full drawn line of the tire shaped ring contribute to the observed scattering intensity, but also those ending within the shaded area

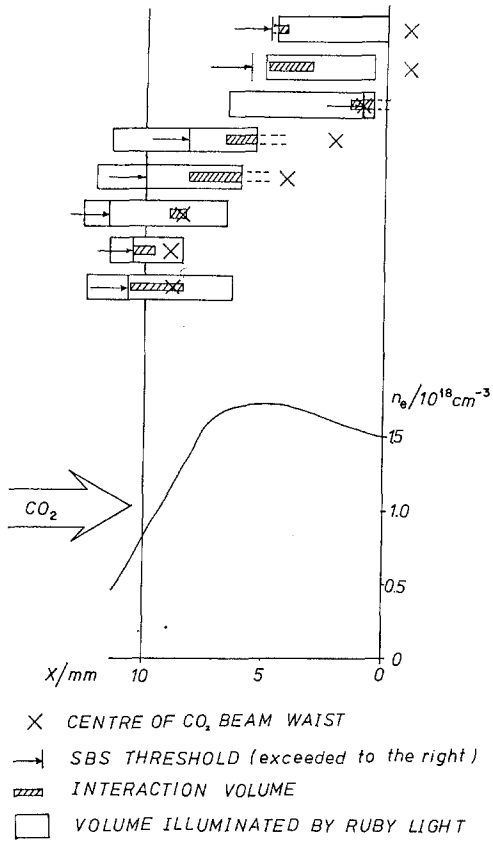

Fig. 4. Location of the SBS interaction volume. The lower part shows the radial density distribution corresponding to the interaction and irradiation volumes of the upper part. The CO_2 laser is incident from the left

synchronisation was achieved between Z-pinch, nanosecond CO_2 laser emission, nanosecond ruby-laser emission and streak camera, suprathermal scattering could be observed on the TV monitor of the streak system. In that way 2-dimensional distributions (showing time and spatial development) of scattering intensity were obtained and were transmitted to a PDP 11-computer for recording and further processing via an optical data transmission link.

2. Experimental Results and Discussions

2.1. Location of the SBS *Interaction Volume*

The radial location of the SBS volume within the Z-pinch plasma was measured by recording suprathermal scattering of ruby-laser light at 7° with the help of the streak camera, the entrance slit of which was aligned to permit the measurement of scattering power along the propagation direction of the SBS excited ion acoustic wave. Since both, the plasma parameters, and the CO_2 laser intensity distribution in the focal waist were known from other investigations [8], the points of SBS threshold indicated by arrows in Fig. 4 could be determined as well as the midplane of the waist distribution indicated by crosses therein. The extension of suprathermal ruby-laser light scattering is represented by the shaded boxes whereas the extension of ruby-laser illumination is visualised by the full drawn boxes. For radial reference also the electron density distribution of the Z-pinch plasma column is plotted in Fig. 4.

Scanning the radial location of the beam waist across the column diameter by shifting the focussing lens, it is clear from Fig. 4 that SBS occured in the dense portion of the plasma and not in the corona. SBS closely follows the location of the CO_2 beam waist. In the density gradient regime an inclination exists for SBS to set in at somewhat above the threshold of an homogeneous plasma (third box from below), a feature which is to be expected from theory [9]. The length of the SBS volume does not extend over the full distance between the points of threshold nor over the whole plasma diameter but its extension varied with the level of SBS backscattering.

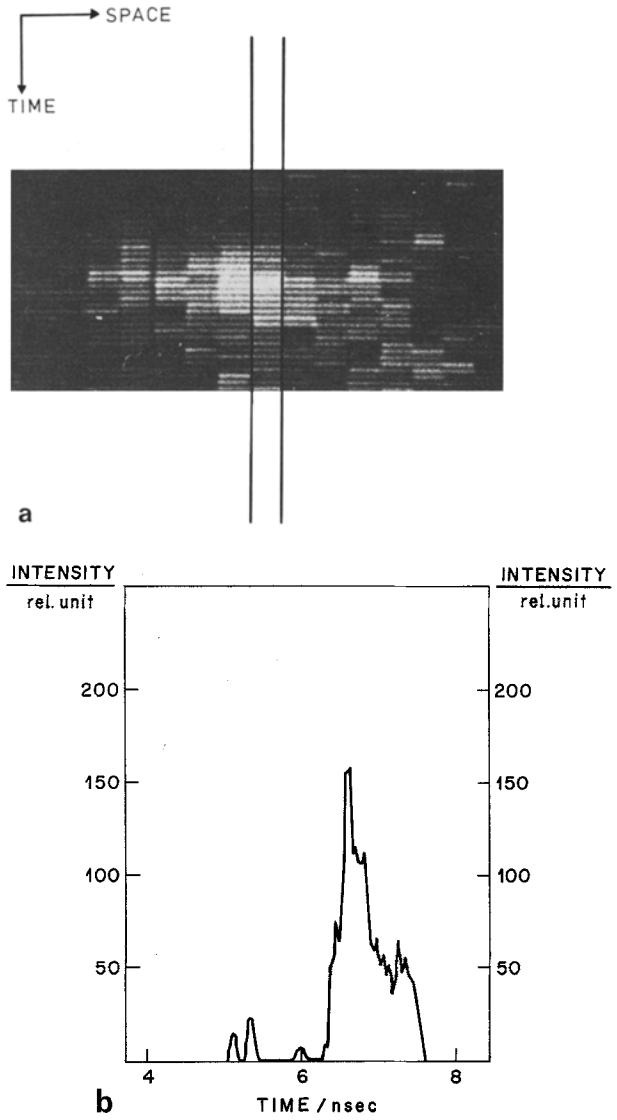

Fig. 5a and b. Typical example for the evaluation of streak camera exposures. The intensity within the vertical bars of (a) is electronically read out and plotted in (b)

2.2. *Spatial Distribution of the Ion Acoustic Wave Amplitude and Length of Interaction Volume*

Provisions were made to operate the streak camera in its linear dynamic range only. In this case, the space and time development of the recorded scattered light intensity is directly proportional to the squared amplitude of the ion acoustic wave. A readout of such a temporal development of wave energy along its propagation direction, denoted here by space coordinate x, is given in Fig. 5b. The x-coordinate was subdivided in 64 readout channels one of which is indicated in the figure by vertical bars and the particular readout for which is also shown in Fig. 5b.

From the digitized readout of the 64 x-channels the space and time evolution of the backscattering ion acoustic wave could be plotted with the help of a PDP 11-computer. As an example the temporal evolution in the central eleven x-channels is represented in Fig. 6.

In Fig. 7a–c sections at the time of maximum ion wave energy (upper curves) and mean values for a 200 ps period about the maximum (lower curve) are represented for different levels of SBS backscattering R. From such sections the length L of the SBS volume was determined. Whereas the steep rise at small x permitted to define the onset of suprathermal ruby-laser light scattering with good accouracy, the flat fall in some cases caused uncertainties up to 50% in L in determining the disappearance of suprathermal scattering intensities.

The dependence of L on the SBS backscatter level R obtained in this way is depicted in Fig. 8. It shows a steady increase of L with R. At only 10% SBS backscattering the ion acoustic wave, i.e. the SBS volume, extends over more than hundred wavelength. For much higher backscattering levels it was necessary to focus the CO_2 laser beam to certain locations within

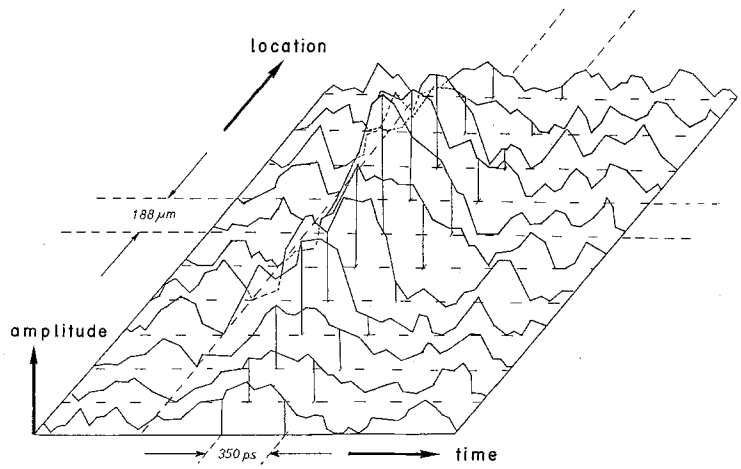

Fig. 6. Example of the space and time dependence of ruby-laser-light scattering intensity. For details see text

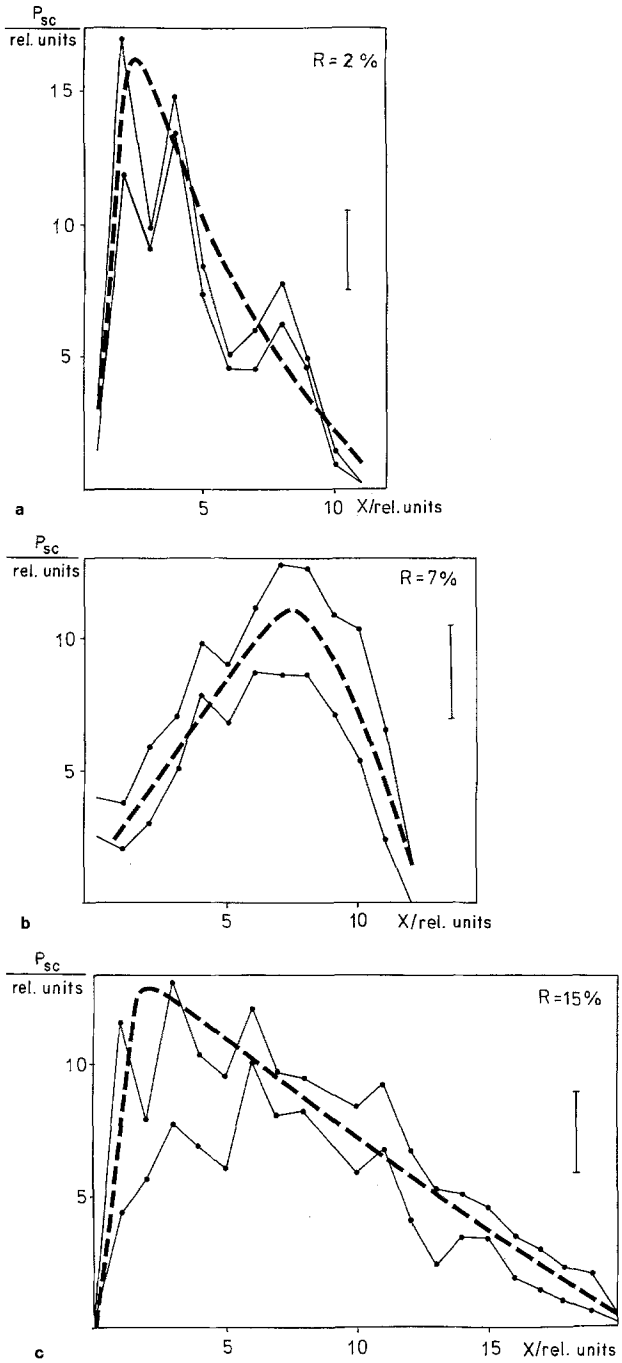

Fig. 7a–c. Spatial distributions of ruby-laser-light scattering intensity for (a) 2% SBS reflection, (b) 7% SBS reflection, (c) 15% SBS reflection. Upper full drawn curves were maintained at time of maximum ion wave energy, lower full drawn curves are mean values for a 200 ps period about this maximum. Also, a vertical error bar is shown in each plot. The dashed curves represent best fit curves used for comparison with computer solutions of the system of Eqs. (7–9)

the plasma column in order to provide for optimum length of the SBS volume on the order of 10 mm. It was in this way, that SBS backscatter levels at the Manley-Rowe limit of near 100% for the maximum CO_2 laser intensity of about 5×10^{16} W/m^2 could be reached.

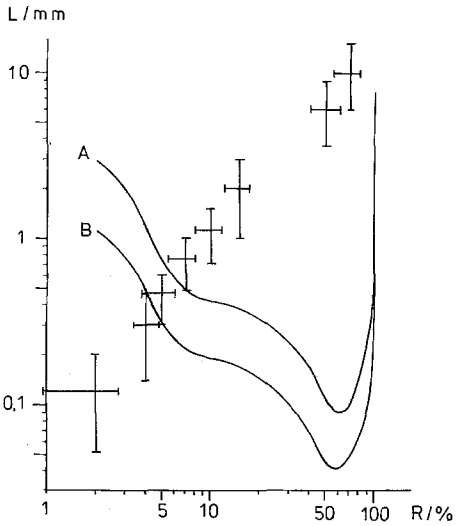

Fig. 8. Dependence of interaction length L on SBS reflectivity R. Also, theoretical curves are shown for the case of high ion wave damping according to the approximate solution of Kruer [14]: Curve A is for a noise level of $\varepsilon=10^{-8}$, Curve B for $\varepsilon=10^{-4}$

2.3. Temporal Development of the Ion Acoustic Wave Amplitude

The streak speed chosen for the measurements of Fig. 6 permitted a temporal resolution of 100 ps. Thus, the steep rise in the vicinity of maximum scattering intensity was resolution limited. In fact, an estimate of SBS growth-rates in an homogenous plasma [8] leads to exponentiation times between 10 and 20 ps. Further, the observation of simultaneous onset and rise must be considered an indication for the SBS to develop in its final phase as an absolute instability. Also, the consistent appearance of peaks before and after this maximum in all x-sections shows the presence of a modulation in the ion wave energy which might be another revelation of modulation caused by ion trapping as has been reported in [10].

3. Evaluation of Measurements

3.1. Theoretical Description

Forslund et al. [11] have derived a coupled system of differential equations for the vector potentials of the SBS waves in an homogeneous plasma. In dealing only with amplitude variations long compared to wavelength, the nonlinear treatment of the system of wave equations can be simplified to give

$$\frac{|c_{ia}|}{c_0}\left(\frac{\partial y_0}{\partial\tau}+\beta_0 y_0\right)+\frac{\partial y_0}{\partial\xi}=yy_-\,, \tag{1}$$

$$\frac{|c_{ia}|}{c_-}\left(\frac{\partial y}{\partial\tau}+\beta_- y_-\right)+\frac{\partial y_-}{\partial\xi}=y_0y^*\,, \tag{2}$$

$$\frac{\partial y}{\partial\tau}+\beta y+\frac{\partial y}{\partial\xi}=y_0y_-^*\,. \tag{3}$$

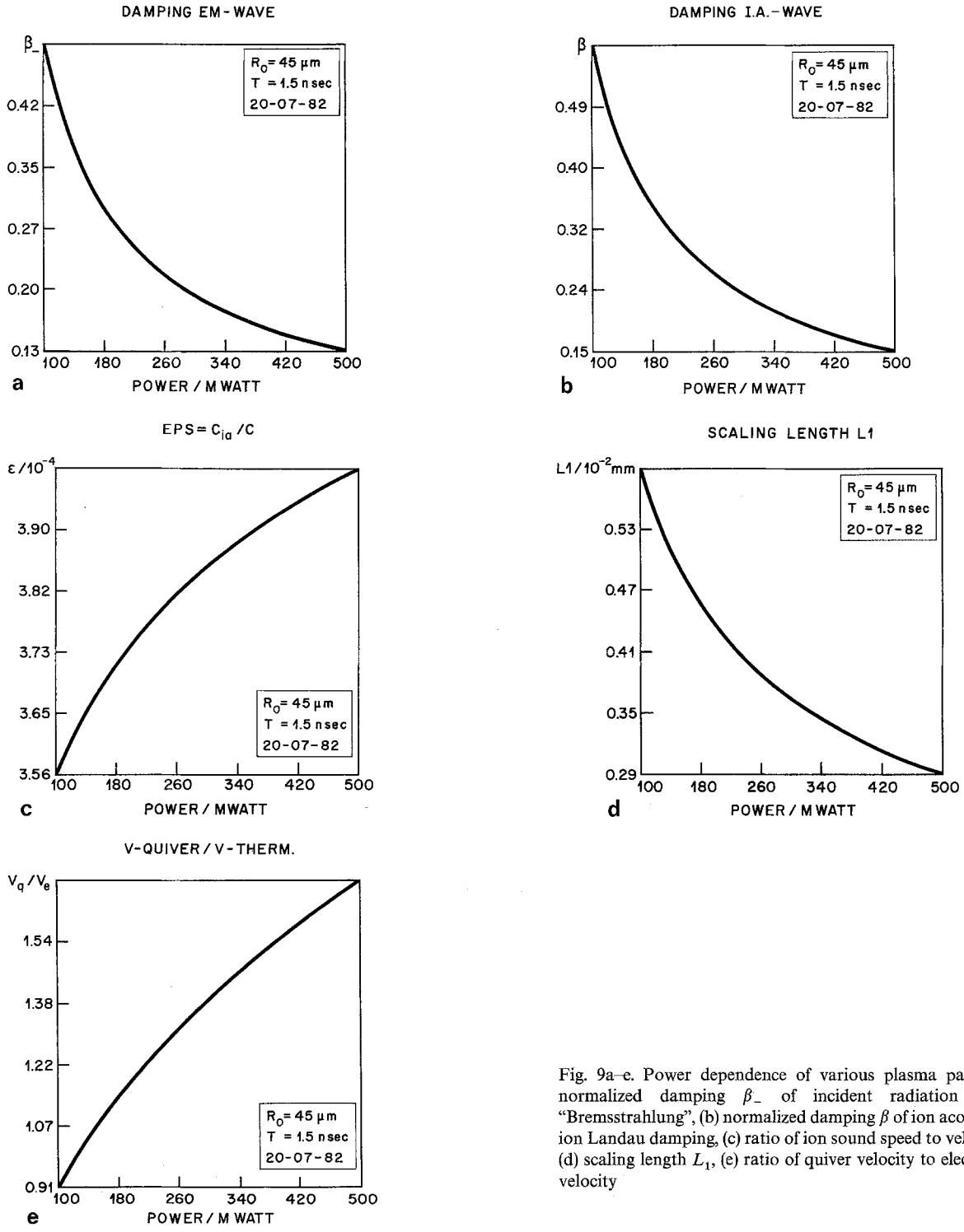

Fig. 9a–e. Power dependence of various plasma parameters: (a) normalized damping β_- of incident radiation by inverse "Bremsstrahlung", (b) normalized damping β of ion acoustic wave by ion Landau damping, (c) ratio of ion sound speed to velocity of light, (d) scaling length L_1, (e) ratio of quiver velocity to electron thermal velocity

Here, $y_{0,-}=A_{0,-}(x,t)/A_0(0,0)$ are the normalized vector potentials of the electromagnetic waves, $y=|K_0\cdot c_{ia}|\cdot A_p(x,t)/|K_p\cdot c_0|\cdot A_0(0,0)$ is the normalized vector potential of the ion acoustic wave, $c_{0,-,ia}$ are the phase velocity of the respective waves, $\xi=x/L$, and $\tau=t/T_1$ are the normalized space and time variables, $L_1=|c_{ia}c|^{1/2}/\gamma_0$ and $T_1=L_1/c_{ia}$ are the scaling length and time, γ_0 is the linear growthrate, $K_{0,p}$ are coupling factors of electromagnetic or ion acoustic vector potentials, respectively, $\beta=L_1\cdot\Gamma/c_{ia}$ is the normalized damping of the ion acoustic wave with damping rate Γ, $\beta_{0,-}=L_1\cdot\Gamma_{0,-}/c_{0,-}$ are the normalized damping of

the electromagnetic wave with damping rates $\Gamma_{0,-}$, and * denotes the complex conjugate.

Since all the specific plasma and laser parameters were known during the laser plasma interaction process [7d], the scaling quantities necessary for a comparision with theory could be determined. The important ones are given in Fig. 9a–e for the conditions of spatial and temporal maxima in the ion wave energy. Γ_- was set equal to inverse "Bremsstrahlung" absorption according to (4), whilst ion Landau damping was used for Γ_p using (6):

$$\Gamma_- = \nu_{ei}\frac{\omega_{pe}^2}{2\omega_0^2}, \tag{4}$$

where ω_{pe} is the electron plasma frequency and

$$\nu_{ei} = Z\cdot n_e \ln\Lambda_c\cdot(k_B\cdot T_e)^{-1.5}\, 4.2\times 10^{13}\,\mathrm{s}^{-1} \tag{5}$$
$$(k_B\cdot T_e \text{ in eV and } n_e \text{ in cm}^{-3})$$

is the electron ion collision frequency given in [12].

Ion Landau damping was formulated for $T_e/T_i < 10$ by a relation approximating the numerical solutions very satisfactorily [13]

$$\Gamma_p = 1\cdot 1\cdot\omega_{ia}\cdot\left(\frac{T_i}{Z\cdot T_e}\right)^{1.75}\cdot\exp\left[-\left(\frac{T_i}{Z\cdot T_e}\right)^2\right]. \tag{6}$$

The curves in Fig. 9 are given for a fully ionized target plasma the initial conditions of which are $n_e = 1.6\times 10^{24}\,\mathrm{m}^{-3}$ and $k_B T_e = k_B T_i = 10\,\mathrm{eV}$ and which is heated by a CO_2 laser pulse of 1.5 ns (FWHM) duration and a focal spot diameter (e^{-2}-power points) of 90 μm within which the power was contained that is given on the abscissas.

For the purpose of trying to explain the experimental results in the framework of the above theoretical description, numerical solutions of the system of Eqs. (1–3) were not required as long as the spatial distribution of ion wave energy was to be compared only for the quasi-stationary state about the time of maximum SBS. In this case the time derivatives in (1–3) can be dropped to leave the following system of coupled equations:

$$\frac{|c_{ia}|}{c_0}\beta y_0 + \frac{\partial y_0}{\partial\xi} = y y_-, \tag{7}$$

$$\frac{|c_{ia}|}{c_-}\beta_- y_- + \frac{\partial y_-}{\partial\xi} = y_0 y^*, \tag{8}$$

$$\beta y - \frac{\partial y}{\partial\xi} = y_0 y_-^*. \tag{9}$$

Because $c_{ia}\beta_0/c_0 \approx c_{ia}\beta_-/c_-$ is on the order of 10^{-3}–10^{-4} the associated quantities could be neglected, in general. As boundary conditions the following values were chosen to suit the experimental situation:

$$y_0(0) = 1$$
$$y_-(0) = R^{1/2} \tag{10}$$
$$y(L) = \varepsilon,$$

where R is the relative SBS power and ε the initial amplitude of the ion acoustic wave.

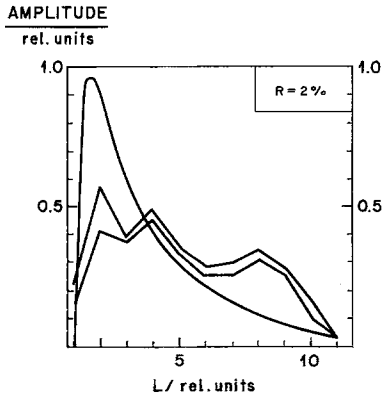

Fig. 10. Numerical solution of Eqs. (7–9) for $R=0.02$, $\beta=5.58$, $\varepsilon^2=10^{-8}$, $\beta_-=0$ drawn as smooth curve. Also shown are the measured amplitude distributions of Fig. 7a

3.2. *Comparison Between Experiment and Theory Regarding Spatial Distribution of Ion Wave Energy*

After the reliability of numerical solutions had been verified by reproducing the solutions given in [11] the spatial distribution of ion wave energy was computed for the various experimental conditions. In Fig. 10 this theoretical curve is plotted for comparison with the experimental distribution of Fig. 7a. It is evident that only a qualitative agreement is achievable, i.e. there is a steep rise on the front side of the interaction volume and a tapering off towards its end with the position of the peaks about coinciding. However, while there is at least such a qualitative agreement at the backscattering level of 2%, the agreement is diverging rapidly for higher levels.

The measured extension of the interaction volume (Fig. 8) becomes so long that solutions of the system of (7–9) are only possible if the ion wave damping is assumed to exceed considerably ion Landau damping. In order to achieve better agreement between theory and experiment ion Landau damping was replaced by a free damping parameter β_{eff}, the value for closest approach of which is plotted in Fig. 11 as a function of backscattering level R. Since the experimental values of L and of other parameters are associated with errors, also the β_{eff} cover a range of uncertainty which is shaded. It is interesting to note that, well below 5% SBS level, this β_{eff} coincides with ion Landau damping

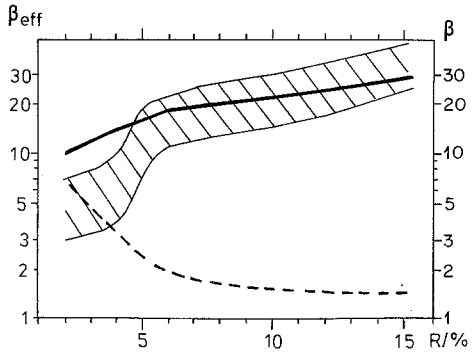

Fig. 11. Phenomenological damping β_{eff} that is necessary to account for the measured experimental values, if the system of Eqs. (7–9) is applied (shaded region). The full drawn line corresponds to an approximation of $\beta_{eff}=\kappa R^{1/2}$ (Sect. 4.7), whereas the dashed line shows the ion Landau damping parameter β

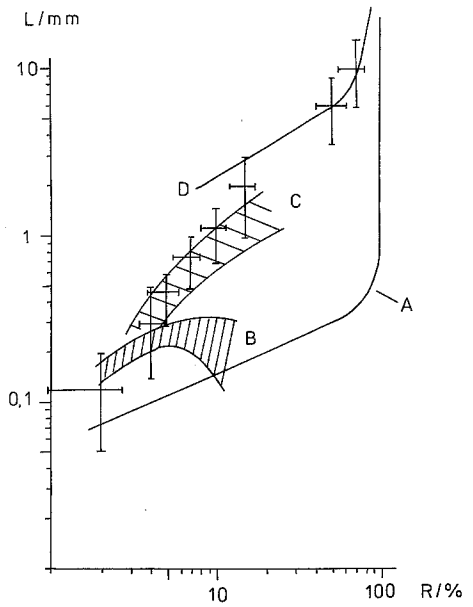

Fig. 12. Comparison of the measured interaction length with theoretical models. (A: ion trapping model [16], B: region of numerical solution of Eqs. (7–9) with only ion Landau damping, C: numerical solution of (15–18) for the case of production of the first harmonic ion wave with the boundary values given by the experiment, and D: approximation for harmonic production in the case of weak damping of the harmonic wave)

(dashed line) whereas the divergence becomes obvious just at those levels about 5% for which the steep increase of SBS with incident CO_2 laser intensity also exhibits a sharp bend [1, 10]. Even though solutions could be obtained at all by the introduction of this free parameter β_{eff}, they showed the worse agreement with experimental distributions the higher the SBS level exceeded the ominous 5%. These observations can be considered an indication for the right direction to go in order to improve the agreement between theory and experiment. The situation calls for higher damping of the ion acoustic wave.

The pronounced onset of additional damping at high ion wave amplitude must be understood as the revelation of another nonlinear mechanismn.

The fact, that the incorporation of a free β_{eff} into the system of Eqs. (7–9) cannot remedy the poor coincidence of measurements and theoretical prediction, shows, that the mere three-wave equations (1–3) or (7–9) at higher SBS levels do not suffice to describe the physical situation correctly.

This inability becomes even more obvious in the extent to which the measured interaction length L is at variance with the predictions of this description. In Fig. 8, Curves A and B represent approximate solutions for high ion wave damping and for the ansatz $y_-^2=y_0^2-T+\tilde{\varepsilon}$ (T transmitted intensity) which results in [14]:

$$R(1-R)=\tilde{\varepsilon}\exp[gL(1-R)], \tag{11}$$

where

$$g=\frac{1}{4}\frac{n_e}{n_c}\cdot k_0\cdot\left(\frac{v_q}{v_e}\right)^2\left[\frac{\Gamma_p}{\omega_{ia}}\left(1+3\frac{T_i}{T_e}\right)\right]^{-1}\cdot\left(1-\frac{n_e}{n_c}\right)^{-1/2}$$

($\tilde{\varepsilon}$: the noise level of $|y|^2$ at the end of the interaction volume from where it grows, L: length of interaction volume, k_0: wave vector of incident radiation, n_e/n_c: electron density n_e normalized to the critical density n_c, v_q/v_e: electron quiver velocity normalized to its thermal velocity, Γ_p/ω_{ia}: ion Landau damping normalized to ion wave frequency, and T_e/T_i: ratio of electron to ion temperature.)

By contrast to the above approximate solution A and B of Fig. 8 the shaded region B in Fig. 12 represents the exact numerical solutions of the system of Eqs. (7–9) for a range of R for which the approximations do not apply so well. Obviously, they are also at variance with the observed behaviour of the interaction length L as R transgresses the ominous limit of about 5%. However, before improvements in the description are considered in Sect. 4, a comparison between another dependence and the predictions of this three-wave theory should be interlaced in the hope to gain additional hints on the possible mechanism.

3.3. Comparison of Experiment and Theory Regarding the Dependence of Ion Wave Amplitude on SBS *Level*

With the knowledge of plasma and laser parameters and the interaction length L, the relative density amplitude of the backscattering ion wave $\delta n_{ia}/n_e$ can be evaluated from solutions of the system of Eqs. (7–9).

On the other hand, for backscattering well below 100% an analytical relation can be derived [15]

$$\left\langle \frac{\delta n_{ia}}{n_e} \right\rangle = 3.5 \tanh^{-1}(R^{1/2})/L \quad (L \text{ in mm}). \tag{12}$$

This relation permits to determine the space averaged quantity from measurements of the relative backscattering level R, if the interaction length L is known. In Fig. 13 such experimental values of $\langle \delta n_{ia}/n_e \rangle$ are covering the shaded region the width of which is caused mainly by the uncertainties in L as far as the higher R region is concerned, and predominantly by the uncertainties in R as for values below 5%.
Solutions of the three-wave equations (7–9) cover the even wider region which is dotted. They react most sensitively to the uncertainties in plasma and laser parameters and, thus, render themselves useless for the intended comparison. Also indicated are experimental values derived from 7° ruby-laser light scattering (points with error bars). In principle, this technique could have provided the same information, however, due to the higher absolute errors encountered here the evaluation from CO_2 backscattering was preferred. Nevertheless, also the technique confirms the experimental values. In Fig. 13 also the upper limit for $\langle \delta n_{ia}/n_e \rangle$ is plotted. A relation for this limit was given by Dawson [16] on the basis of ion trapping in a "waterbag model" leading to

$$\frac{\delta n_{ia}}{n_e} = 0.5\left[\left(1+\gamma_{ia}\frac{T_i}{T_e}\right)^{1/2} + \left(3\frac{T_i}{T_e}\right)^{1/2}\right]^2. \tag{13}$$

With the exception of very small values of R one can see that $\langle \delta n_{ia}/n_e \rangle$ stays well below this limit at which additional nonlinear wave damping would occur. For this reason ion trapping can be excluded already as the nonlinear damping mechanism to be sought above 5% in R.
$\langle \delta n_{ia}/n_e \rangle$ assumes only values on the order of percent. More surprising, however, is the feature that it decreases while the backscattering increases. The solution to this paradoxial behaviour is provided by the measured dependence of the interaction length L on R represented in Fig. 8. The steady increase of L with R is overcompensating the slight decrease in the density amplitude of the backscattering ion wave. This might be a result of greater significance. On one hand, it explains, why the Manley-Rowe limit of SBS could be reached in this plasma [1] – in more or less contrast to all other model experiments – and even at moderate CO_2 laser intensities. With more than 10 mm extension the homogeneous plasma was long enough not to chop off essential portions of the interaction volume developing in such an homogenous plasma.

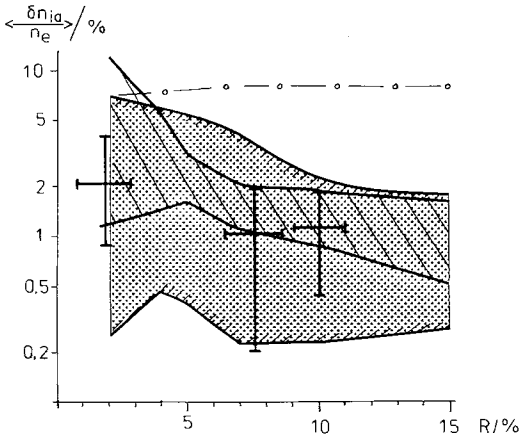

Fig. 13. Relative density amplitude of the backscattered ion wave $\delta n_{ia}/n_e$ as a function of SBS reflectivity. The shaded region is an analytical solution of Eqs. (7–9) for high damping. The exact numerical solution of (7–9) for the experimentally observed boundary conditions is shown as the dotted area. The experimental values are derived from the height of the spectrally integrated ruby scattered intensity under 7°. Also an upper limit (—o—o—) is shown given by the ion trapping model [16]

On the other hand, this result may represent serious implications for larger laser-fusion targets the underdense corona of which will expand over several millimeters during nanosecond irradiation. In these experiments similar conditions for the development of SBS are created. Even worse, since not the length itself counts but the number of wavelengths fitting in it, wavelengths shorter than that of the CO_2 laser should be affected much more. The hope, that at the higher laser intensities of fusion targets the beneficial effects of nonlinear mechanisms would provide sufficient relief, obviously does not obtain. For instance, it was demonstrated at CO_2 laser intensities comparable to those in the corona of laser fusion targets, that, with a plasma length of a few millimeters only, SBS assumed values in excess of 50% [26]. Even in case of rather inhomogenous plasmas produced and irradiated by a Nd laser [17] that decisive role of plasma length made itself felt.

4. Discussion of Nonlinear Damping Mechanisms

The poor agreement between experiment and the predictions of the three wave treatment in Sect. 3 hint at the contribution of a damping mechanism, in addition to linear ion Landau damping. It must be a nonlinear mechanism, because its influence becomes pronounced only at high ion wave amplitudes corresponding to about 5% backscattering level. As has been done in greater detail in [15, 18], a number of likely candidates is reviewed and discussed to single out a process capable to explain the SBS behaviour well above threshold.

4.1. Ion Heating

The idea is, that associated with ion trapping a heating of ions occurs which increases ion Landau damping. Without going into details, which can be found in [14] or [15, 18], this possibility can be rejected for reasons that the measured density amplitudes of the ion wave are nearly an order of magnitude below the limit for strong ion trapping and, therefore, the associated heating cannot occur.
Even, if there were another process transferring wave energy to the ions, the plasma conditions are such, that it would take 10 ns to thermalise this energy as compared to the 1 ns the ion wave exists. Last but not least, an essential increase of ion temperature could not be observed in the course of a light scattering investigation of the interaction volume [7d].

4.2. Ion Trapping

As pointed out above the measured ion wave amplitudes are about an order of magnitude too small for essential ion trapping to occur.
Even if this fact would be ignored and the ion trapping limit of $\delta n_{ia}/n_e$ given by (13) were used for the evaluation of L as a function of R a great discrepancy between this relation (Fig. 12, Curve A) and experimental values becomes evident, again disproving this possibility.

4.3. Energy and Momentum Transfer to the Plasma

If the ratio of quiver velocity v_q of the electron to its thermal velocity v_e exceeds unity, plasma acceleration can be caused by light pressure instead of plasma pressure causing additional damping to the waves. This possibility has been dealt with by Kruer et al. [19]. However, corresponding conditions were only prevailing in the plasmas at backscattering levels above 50%, whereas a process is sought for, which is greatly increasing the damping already from 5% on. It can, thus, also be discarded.

4.4. Pump Depletion

For reasons of energy conservations the pump wave amplitude cannot stay constant in the interaction volume, if the backscattered wave assumes comparable amplitudes. As a consequence, amplitude and frequency modulation occurs associated with a redshift of the backscattered wave [11]. Apart from the fact that this redshift could not be observed in the plasma for the conditions of strong additional damping [18], this process cannot be expected to make itself strongly felt already at 5% backscattering and must not be considered, either.

4.5. Rescattering

As long as the backscattered wave exceeds the SBS threshold it can be backscattered again within the plasma and so forth. The simplest use of only one rescatter was dealt with by Karttunen [20a] and Speziale et al. [20b], and leads to saturation of SBS backscattering at a level of 62%. Such an SBS saturation was not observed for the plasma investigated [1] and the double red-shifted component could not be seen in forward direction [18]. Also this mechanism, thus, cannot have caused the additional damping.

4.6. Wave Decay and Ion Turbulence

Since the ion wave frequency is far below the ion plasma frequency, the dispersion disappears and the decay of the ion wave in daughter waves is possible with only obeying energy and momentum conservation. The production of two waves of equal frequency has the highest probability and the wavenumber $k_{1/2}=k_{ia}/2$ has maximum growth rate according to Karttunen and Salomaa [21]. This growth rate γ_{ia} normalized to that of SBS in an homogeneous plasma is given in [21] by

$$\gamma_{ia}/\gamma_{\mathrm{SBS}} \approx \left(2\frac{m_e}{m_i}\right)^{1/2} \cdot \left(\frac{\omega_0^3}{\omega_{pe}\cdot k_{ia}\cdot c_{ia}}\right)^{1/2} \cdot |A_p| \cdot |A_0| . \qquad (14)$$

For the conditions of the plasma investigated $\gamma_{ia} \ll \gamma_{\mathrm{SBS}}$ and this process should not play a significant role. Also from another reason this possibility must be rejected. Extensive numerical calculations [21] lead to the result that saturation due to this process should limit SBS to below 10% which is greatly at variance with the observation of the Manley-Rowe limit near 100% [1]. Finally, because this primary ion wave decay is impeded, the subsequent decay and spread of daughter waves cannot proceed to fill the k-space in a manner required for the state of ion turbulence and hence ion turbulence can be discarded, too.

4.7. Ion Wave Harmonics and Wave Breaking

As long as the ion wave frequency is very small compared to the ion plasma frequency, harmonics caused by nonlinear wave effects propagate at nearly the same phase velocity as their source terms associated with the high amplitude fundamental wave. As a consequence of this phase-matched feeding, the harmonic waves can assume considerable amplitudes, the general conditions for which have been given, for instance, by Franklin [22]. A detailed theoretical treatment of such harmonics production was carried out by Karttunen and Salomaa [23], and Gellert [24]. The process has been confirmed in experiments perfor-

med in the microwave region by various groups [25].

In formulating only the simplest case of the production of the first harmonic wave at $(2\omega_{ia}, 2k_{ia})$ the system of coupled wave equations must be extended to include that of the harmonic wave and its mutual coupling with the fundamental ion wave. The system then reads

$$\frac{|c_{ia}|}{|c_0|}\left(\frac{\partial y_0}{\partial\tau}+\beta_0 y_0\right)+\frac{\partial y_0}{\partial\xi}=yy_-\,, \tag{15}$$

$$\frac{|c_{ia}|}{|c_-|}\left(\frac{\partial y_-}{\partial\tau}+\beta_- y_-\right)+\frac{\partial y_-}{\partial\xi}=y_0 y^*, \tag{16}$$

$$\frac{\partial y}{\partial\tau}+\beta y+\frac{\partial y}{\partial\xi}=y_0 y_-^*-\kappa y y_2\,, \tag{17}$$

$$\frac{\partial y_2}{\partial\tau}+\beta_2 y_2+\frac{\partial y_2}{\partial\xi}=\kappa y y^*, \tag{18}$$

where the index 2 refers to the respective quantities of the harmonic wave and the coupling factor

$$\kappa=8\sqrt{2}k_0\omega_0 c_0\omega_{pe}^{-2}\,. \tag{19}$$

This system was solved numerically to render possible a comparison with experimental results. That the inclusion of (18) must have a pronounced effect can be anticipated already from the coupling factor assuming a value of 69 for the conditions of our experiment. In fact, the distribution of ion-wave energy along its propagation direction at the time of peak backscattering being plotted in Fig. 14 in comparison with the measured distribution from Fig. 7b (shaded), shows a distinct deviation from the solution of the three-wave system (compare, e.g., Fig. 10). In addition, it becomes obvious from the comparison that these theoretical predictions are coinciding reasonably well with the observations. One cannot help but conjecture that harmonic production is the physical mechanism sought for.

Of course, this has to be solidified by demonstrating agreement also with respect to other predictions of the model. Thus, numerical solutions of (15–18) were computed for the plasma and laser conditions measured. They are affected by the uncertainties of these parameters to form a band (Fig. 12, Region *C*, shaded). Not being adjusted to the experimental points, they represent absolute values. It is in this way that the very satisfactory agreement with observations receives special weight. In case of negligible damping of the harmonic wave an approximation to the relation between backscattering R and interaction length L can be formulated analytically [23] as

$$(1-R)=\left(\frac{\tilde{\varepsilon}}{4R}\right)^{\sqrt{R}}(1+R)^2\exp[2(1-R)L/\kappa L_1]\,. \tag{20}$$

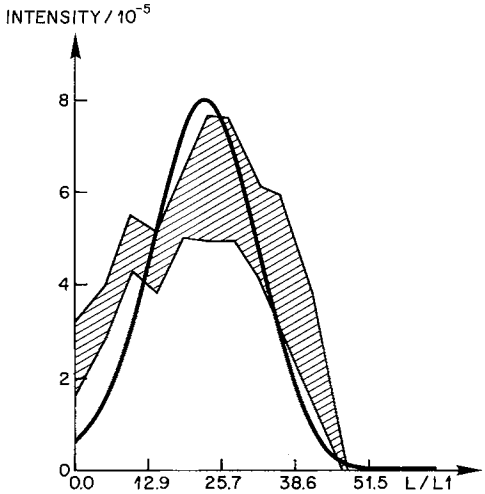

Fig. 14. Numerical solution of (16–19) including production of harmonic ion wave for $R=0.07$, $\beta=1.5$, $\varepsilon^2=10^{-8}$, $\kappa=70$, $\beta_-=0.1$, $(\delta n_{ia}/n_e)(L)=5\times10^{-3}$. The shaded area is the experimentally observed distribution of Fig. 7b

The corresponding curve is plotted in Fig. 12, too. It also demonstrates agreement for the high R values for which the harmonic damping can be expected to satisfy the above assumption due to the increase in the ratio T_e/T_i and for flattening of the ion velocity distribution [27] both lowering Landau damping.

A final proof as to the applicability of this four-wave description is provided by the comparison of effective ion wave damping β_{eff} determined from measurements (Fig. 11) and an approximation $\beta_{\text{eff}}\approx\kappa\sqrt{R}$ derived from this model in [23] for backscattering above about 5%. The agreement shown in Fig. 11 is also highly satisfying.

In view of the various aspects for which a highly satisfactory explanation could be provided by the inclusion of harmonic damping, it must be inferred that this mechanism cannot have been an influence only to be felt under the particular conditions of our experiment, but this phenomenon of harmonic damping must be a more general feature of experiments dealing with SBS. It is therefore, not amazing to find that indeed such harmonic production could be observed directly by means of light scattering techniques in a quite different target plasma [6].

5. Summary and Conclusions

An homogeneous, underdense, and fully ionised plasma of large extension was irradiated with CO_2 laser intensities up to 10^{17} W/m^2 and the resulting SBS was investigated by means of ruby-laser-light scattering techniques complemented by measurements of the backscattered CO_2 radiation. Suprathermal light scattering from the SBS interaction volume recorded with

the help of a fast streak camera permitted to measure the evolution of the backscattering ion wave in the time and in the spatial coordinate of its propagation direction. In analysing these measurements the location of the SBS volume could be shown to lie in the dense plasma column of the Z-pinch rather than in the corona surrounding it. By shifting the focussing lens, SBS could be made to occur in various positions across the column radius. Whereas everywhere in the homogeneous part SBS developed near the locations where the threshold for an homogeneous plasma was exceeded, in the gradient regions the inclination for SBS to set in at higher laser intensities can be inferred. The length of the interaction volume increases with the level of backscattering, i.e. the laser intensity, and, at the Manley-Rowe limit near 100%, becomes comparable with the plasma diameter, so that for maximum backscattering the laser beam waist must be focussed to an optimum position near the plasma center in order to provide maximum length.

The temporal evolution of the backscattering ion wave shows in its final phase simultaneous rise in all positions and the instability must, therefore, be of absolute nature. Also, a periodic modulation of ion wave energy can be recognised from these measurements. It might be associated with ion trapping as has been reported in [10].

For the purpose of comparing various aspects of these experimental observations with theoretical predictions, sections of these distributions were formed for the time of peak backscattering and their dependence on backscattering level R of both the interaction length L and the mean density amplitude of the ion wave were evaluated. The same function of density amplitude on R was also determined from simultaneous measurements of SBS backscattering and ruby-laser-light scattering. The relative amplitude $\delta n_{ia}/n_e$ turns out to assume values not much above one percent even at high backscatter levels and, even more puzzling, the amplitude drops with increasing backscattering. The explanation of this unexpected feature is provided by the above observation that the interaction length, i.e. the length of the backscattering ion wave, increases with backscatter level and overcompensates the decline in wave amplitude. This decisive role of interaction length L has significant implications. It explains why the dangerous Manley-Rowe limit could be reached already at low laser intensities in our experiment [1], in contrast to all other model experiments: it was simply that our plasma was long enough. For larger laser fusion pellets with their underdense and fairly homogeneous corona extending over several millimeters this may cause another serious problem. The hope that at the higher laser intensities of fusion targets the beneficial effects of nonlinear mechanisms would provide relief, obviously does not obtain. For instance, it was demonstrated at CO_2 laser intensities comparable to those in the corona of laser fusion targets, that, with a plasma length of a few millimeters only, SBS assumed values in excess of 50% [26]. Even in case of rather inhomogeneous plasmas produced by Nd lasers by the irradiation of solids [17] that decisive role of plasma length had made itself felt.

For the first attempt to explain observations in the light of theories applicable to an homogeneous plasma, the extensive treatment of Forslund et al. [11] was used, the predictions of which had proved capable of describing the observations near threshold in this plasma [1, 8b]. Steady-state solutions of this system of coupled wave equations again were capable to describe at least qualitatively several aspects of the observations for backscattering levels below 5%. This limit between about 5% and 10%, however, came not as a surprise since it was at this level that the further increase of SBS with laser intensity greatly deviated from the initial rapid rise. An attempt to improve agreement between theory and experiment by treating the ion wave damping as a free best fit parameter rather than to fix it by ion Landau damping, was not fully successful, but gave a hint at what was lacking in the above description, namely a nonlinear and additional damping mechanism of the ion wave. Based on experiment [18], computations [15], and estimates, all such mechanisms could be excluded with the exception of one, namely harmonics production of the ion wave. Complementing the above system of wave equations by only that of the first harmonic wave permitted to obtain satisfying agreement in the aspects checked. These were the dependences of interaction length L and the effective damping of the ion wave β_{eff} on the level of backscattering R. In addition, it explains the high damping of the ion wave at its density amplitudes which are far below the limit of ion trapping. This system of four-wave equations is also capable to explain the SBS instability at damping values well in excess of $\beta = 2$, the limit for absolute instability given by the three-wave model.

It is in this way, that a theoretical treatment was found capable of describing satisfactorily the conditions of experiments with homogeneous and underdense plasmas of large extent. This might also imply additional problems for larger laser fusion targets the corona conditions of which are comparable with those investigated.

It is pointed out in this context that, contrary to other laser-fusion aspects, for a given plasma length the implications are the more serious the *shorter* the laser wavelength is.

Acknowledgements. Excellent cooperation with Dr. J. Handke is gratefully acknowledged. The authors are thankful to Dr. D. Rusbüldt of the IPP, Kernforschungsanlage Jülich GmbH, D-5170 Jülich, Fed. Rep. Germany for supplying valuable advise and hardware. Also, our appreciation for discussions on theoretical aspects with Prof. Dr. H. Schamel must be expressed, here. Finally, thanks must be given to Mrs. Zamfirescu for preparing the drawings with greatest care.
This research was performed under the auspices of the "Sonderforschungsbereich No. 162, Plasmaphysik Bochum/Jülich."

References

1. J. Handke, S.A.H. Rizvi, B. Kronast: Appl. Phys. **25**, 109 (1981)
2. a. A.A. Offenberger, A. Ng., M.R. Cervenan: Can. J. Phys. **56**, 381 (1978)
   b. A. Ng., A.A. Offenberger, S.J. Karttunen: Opt. Commun. **36** (3), 200 (1981)
   c. A. Ng., L. Pitt, D. Salzmann, A.A. Offenberger: Phys. Rev. Lett. **42**, 307 (1979)
   d. R. Giles, A.A. Offenberger: Phys. Rev. Lett. **50**, 421 (1982)
3. a. M.J. Herbst, C.E. Clayton, F.F. Chen: Phys. Rev. Lett. **43**, 1591 (1979)
   b. J.J. Turechek, F.F. Chen: Phys. Fluids **24**, 1126 (1981)
   c. C.E. Clayton, C. Joshi, A. Yasuda, F.F. Chen: Phys. Fluids **24**, 2312 (1981)
4. a. R.S. Massey, Z.A. Pietrzyk, D.W. Scudder: Phys. Fluids **21**, 396 (1978)
   b. R.S. Massey, K. Berggren, Z.A. Pietrzyk: Phys. Rev. Lett. **36**, 963 (1976)
   c. Z.A. Pietrzyk, T.N. Carlstrom: Appl. Phys. Lett. **35**, 681 (1979)
5. C.J. Walsh, J. Meyer, B. Hilko: Appl. Phys. Lett. **38**, 82 (1981)
6. C.J. Walsh, H.A. Baldis: Phys. Rev. Lett. **48**, 1483 (1982)
7. a. G. Bertschinger: Dissertation, Ruhruniversität Bochum (1980)
   b. K.H. Finken, G. Bertschinger, S. Maurmann, H.J. Kunze, J. Quant: Spectrosc. Radiat. Transf. **20**, 467 (1978)
   c. K.H. Finken, G. Bertschinger, R.S. Hornady: Z. Naturforsch. **31a**, 1318 (1976)
   d. B. Gellert, B. Kronast: Appl. Phys. B **32**, 175 (1983)
8. a. J. Handke: Dissertation, Ruhruniversität Bochum (1982)
   b. J. Handke: Report 82-N3-109 (1982), Sonderforschungsbereich No. 162, Plasmaphysik Bochum/Jülich, Ruhruniversität D-4630 Bochum, Fed. Rep. Germany
9. C.S. Liu, M.M. Rosenbluth, R.B. White: Phys. Rev. Lett. **32**, 697 (1973)
10. J. Handke, S.A.H. Rizvi, B. Kronast: Phys. Rev. Lett. (accepted for publication)
11. D.W. Forslund, J.M. Kindel, E.L. Lindman: Phys. Fluids **18**, 1002 (1975)
12. a. L. Spitzer, Jr.: *Physics of Fully Ionized Gases* (Interscience, New York 1961)
    b. L. Spitzer, Jr., R. Härm: Phys. Rev. **89**, 977 (1952)
13. F.F. Chen: University of California, Los Angeles, CA 90024 (private communication)
14. W.L. Kruer: Phys. Fluids **23**, 1273 (1980)
15. B. Gellert: SFB-Report 82-N3-109, Ruhruniversität Bochum (Dec. 1982)
16. J.M. Dawson, W.L. Kruer, B. Rosen: In *Dynamics of Ionized Gases*, ed. by M. Lighthill, I. Imai, H. Sato (University of Tokyo Press, Tokyo 1973) p. 47
17. B.H. Ripin et al.: Phys. Rev. Lett. **39**, 611 (1977)
    D.W. Phillion et al.: Phys. Rev. Lett. **39**, 1529 (1977)
    W.L. Kruer: Comments Plasma Phys. Contr. Fusion **4**, 13 (1978)
18. S.A.H. Rizvi: Dissertation, Ruhruniversität Bochum (1983)
19. W.L. Kruer, E.J. Valeo, K.G. Estabrook: Phys. Rev. Lett. **35**, 1076 (1975)
20. S.J. Karttunen, R.R.E. Salomaa: Plasma Phys. **21**, 247 (1979)
    T. Speziale, J.F. McGrath, R.L. Berger: Phys. Fluids **23**, 1275 (1980)
21. S.J. Karttunen, R.R.E. Salomaa: Phys. Lett. **72A**, 336 (1979)
    S.J. Karttunen: Plasma Phys. **22**, 151 (1981)
22. R.N. Franklin: Rep. Prog, Phys. **40**, 1369 (1979)
23. S.J. Karttunen, R.R.E. Salomaa: Phys. Lett. **88A** (7), 350 (1982)
24. B. Gellert: Phys. Lett. **96A**; 16 (1983)
25. N. Sato: Phys. Fluids **13**, 2198 (1970)
    T. Ohnuma, Y. Hatta: J. Phys. Soc. Jpn. **29**, 1597 (1970)
    L.P. Mix, L.N. Litzenberger, C. Bekefi: Phys. Fluids **15**, 2020 (1972)
26. N.H. Burnett: J. Appl. Phys. **48**, 3727 (1977)
27. R. Sugihara, T. Kamimura: J. Phys. Soc. Jpn. **33**, 206 (1972)